Korean J. Chem. Eng.
DOI: 10.1007/s11814-014-0133-0

Korean Journal of Chemical Engineering
October 2014, Volume 31, Issue 10, pp 1845-1858

pISSN: 0256-1115
eISSN: 1975-7220

Predictions of wet natural gases condensation rates via multi-component and multi-phase simulation of supersonic separators

Seyed Heydar Rajaee Shooshtari and Akbar Shahsavand†

Department of Chemical Engineering, Faculty of Engineering, Ferdowsi University of Mashhad, Mashhad, Iran
(*Received 1 December 2013 • accepted 7 May 2014*)

Abstract−Proper correction of water and heavy hydrocarbon dew points of sweet natural gases is essential from various technical and economical standpoints. Supersonic separators (3S) are proved to be capable of achieving these tasks with maximum reliability and minimal expenses. The majority of the previous articles have focused on the flow behavior of pure fluids across a 3S unit. Multicomponent fluid flow inside 3S accompanied with condensation phenomenon will drastically increase the complexity of the simulation process. We tackle this issue by considering a proper combination of fundamental governing equations and phase equilibrium calculations to predict various operating conditions and composition profiles across two multi-component and multi-phase 3S units. Various Iranian sweet gases are used as real case studies to demonstrate the importance of 3S unit practical applications. Simulation results clearly illustrate the effectiveness of 3S units for faithful dehydration of various natural gases, while successfully controlling its dew point, suitable for any practical applications. Conventional HYSYS simulation software is used to validate the simulation results.

Keywords: Supersonic Separator, Natural Gas, Dew Point Correction, Condensation, Flash Calculation

INTRODUCTION

Novel supersonic separators (3S units) are proved to be beneficial for many gas conditioning applications such as combined dehumidification and extraction of heavy hydrocarbons from various natural gases. Water and heavy hydrocarbon dew point corrections are essential for proper transportation and economical aspects. Furthermore, 3S units are reported to have other potential applications, including separation of carbon dioxide and hydrogen sulfide from natural gases and production of liquefied natural gas (LNG) [1].

Traditionally, refrigeration, membrane, adsorption and absorption processes are used as conventional processes for water and hydrocarbon dew point corrections. These processes are usually expensive and require large operational facilities, including complex systems with many adverse environmental effects due to the use of various chemical compounds [2]. Supersonic separators can eliminate a variety of impurities from various natural gas streams in a single compact device. It is reported to enjoy astonishingly high reliability as large as 99% due to the lack of any moving device [3]. In contrast to other conventional separators, the inlet gas stream may enter the 3S unit as a single phase stream. Then two or more phases can be created due to the condensations of water or heavier hydrocarbon species inside the device at extremely low temperatures resulted from adiabatic expansion. This phenomenon can ultimately lead to separation of liquid and gas phases and a single gas stream leaves the 3S unit after proper pressure recovery. Fig. 1 clearly illustrates this issue.

Twister BV (Netherlands) engineers pointed out various potential applications of supersonic separators including natural gas dehydration, hydrocarbon dew point control, deep liquid recovery and hydrogen sulfide removal [1,4-6].

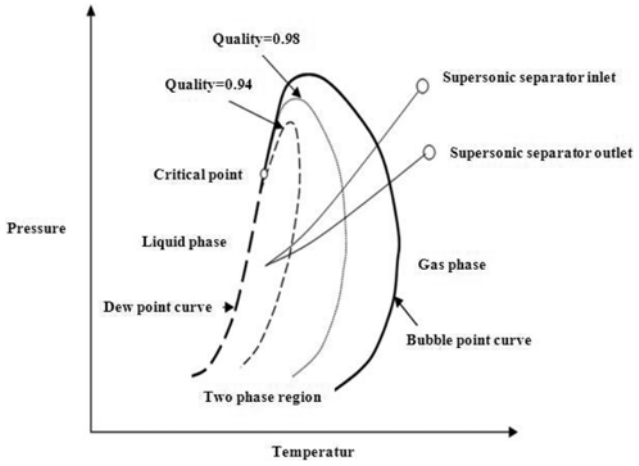

Fig. 1. Typical phase envelope of a retrograde natural gas, demonstrating liquid collection potential of a 3S from a single phase gas stream.

Liu et al. [7] described a 3S based natural gas dehydration unit and presented the corresponding structure and its working principles. Their test results for an indoor 3S rig revealed that the pressure loss ratio, the shock wave location and the fluid flow rate had immense effect on the overall dehydration characteristics of the entire process.

Jassim et al. [8,9] studied the flow behavior of high-pressure natural gas in various supersonic nozzles by resorting to computational fluid dynamic (CFD) technique. The effects of real gas property, nozzle geometry and vorticity on the performance of Laval nozzle

†To whom correspondence should be addressed.
E-mail: shahsavand@um.ac.ir

were investigated. They reported that shockwave position can significantly change when the gas is considered as real rather than perfect and although losses in pressure increase due to the inlet swirl flow, but vorticity increases very sharply in the vicinity of the shock.

Malyshkina [10] presented a two-dimensional Euler model for analysis of gas-dynamic parameters under conditions of separation in the region of shock wave and behind it. Karimi and Abdi [2] investigated the shock wave location inside a supersonic separator. A mathematical model was developed to simulate the flow of natural gas through a converging-diverging nozzle. The results of their model were then compared by a computational fluid dynamics model. In 2010, Malyshkina [11] studied the supersonic separator performance for high temperature separation of natural gas into its components. The compositions of gas–liquid mixtures were determined as a function of initial parameters. In 2011 and 2012 Wen et al. [12-15] investigated the effects of the supersonic swirling flow on the radial distribution of various gas flow parameters inside 3S unit. They also studied the effect of shock wave positions, the particle trajectories and separation efficiencies by using the discrete particle method (DPM). Machado et al. [3] compared the technical and economical aspects of using supersonic separator technology with conventional gas treating units. Ghanbari Mazidi et al. [16] examined two pressure recovery scenarios for supersonic separators. They reported that the use of normal shock wave provides more flexibility than the employment of two consecutive nozzle-diffusers, but may fail drastically if the normal shock wave location precedes the liquid collection point.

Most of the above articles investigated the 3S unit performances in the absence of condensation process. Other researches [17-28] focused on pure component or binary condensation inside supersonic Laval nozzle using droplet nucleation and growth equations. The majority of their collected results cannot be easily extended to 3S unit when operating with multi-component fluids. Lingling et al. [29] presented a mathematical model for overall phase equilibrium prediction of multi-component gas separation process inside supersonic separators. Their model used equilibrium flash calculations with known operating parameters such as temperature and pressure in the outlet of 3S unit. They evaluated the performance of a 3S unit with calculating of temperature and pressure in the throat location by considering the isentropic flow between the entrance and throat. Furthermore, the unity value of Mach number at the throat location provided the second equation to compute corresponding temperature and pressure. They claimed that a good design of Laval nozzle should lead to a two-phase flow regime at the throat location. Moreover, the exit concentrations of all species were calculated at the known outlet pressure and temperature of the Laval nozzle. The presented model did not consider the actual nozzle geometry and the corresponding distributions of various operating conditions (especially the concentration profiles of condensable and non-condensable components) across the nozzle - diffuser of the 3S unit.

In our previous article [30] we presented a model which can be used to simulate the multi-component systems when no appreciable interaction exists between the condensed phases. The model predictions were successfully validated with several experimental data borrowed from the literature.

Recently, many researchers have presented or even simply used several smart techniques (such as artificial intelligence techniques) as valuable predictive tools for determination of important parameters in chemical, environmental, and petroleum engineering. Implementation of these integrated intelligent systems can dramatically increase our problem solving capabilities. Mohaghegh used several examples to highlight the importance of using integrated intelligent systems in various oil and gas industry fields [31].

Zendehboudi et al. developed a smart model to forecast gas-oil minimum miscibility pressure (MMP) using a feed-forward artificial neural network (FF-ANN) combined with particle swarm optimization (PSO) technique. They concluded that the PSO-ANN has the greatest impact on MMP value and can successfully predict the MMP value under different situations [32].

Zahedi et al. used an Artificial Neural Networks (ANN) approach for estimation of asphaltene precipitation. Back-propagation learning algorithm was used to train the networks. They applied Levenberg-Marquardt (LM) algorithm to find the optimal configuration (number of neurons in the hidden layer). The performance of the best obtained network was checked by its generalization ability in predicting one-third of the unseen data. They reported that "ANN's results showed the best estimation performance for the prediction of the asphaltene precipitation." ANN model performance was also compared with the Flory-Huggins and the modified Flory-Huggins thermodynamical models. The comparison confirms the superiority of the ANN model [33].

Shahsavand et al. presented an optimal method for training of the regularization network and applied it to several case studies in the field of membrane and adsorption. The regularization network is a special kind of feed-forward artificial neural network which heavily relies on multivariate regularization theory and, unlike many back-propagation networks, enjoys an extremely powerful background [34,35].

In the current article, the new mathematical model based on the combination of fundamental governing equations (continuity, momentum, energy, Mach number and state equation) and corresponding phase equilibrium calculations is presented for prediction of components concentration along supersonic Laval nozzle axis. The comparison of our simulations results with compatible computations performed using the well known HYSYS simulation software, clearly shows that the presented model can be successfully used as an accurate and powerful tool to predict the performance of a 3S unit for proper separation of various impurities from multi-component natural gas streams.

Evidently, the HYSYS simulation software considers the entire 3S unit as a black box and cannot provide reliable predictions for temperature, pressure, gas velocity and many more operating condition profiles across 3S Laval nozzle. For validation purposes, the temperature and pressure profiles will be initially predicted via our model and then a few points of the profile will be used by HYSYS software to predict the composition profile across the 3S unit by resorting to flash calculations. Finally, the computed profile computed with our model will be compared with HYSYS predictions.

A BRIEF DESCRIPTION OF 3S UNIT

Fig. 2 illustrates that the Laval nozzle plays a critical role in the structure of supersonic separators (3S units), especially before the liquid collection point. The gas enters the swirling section (plenum

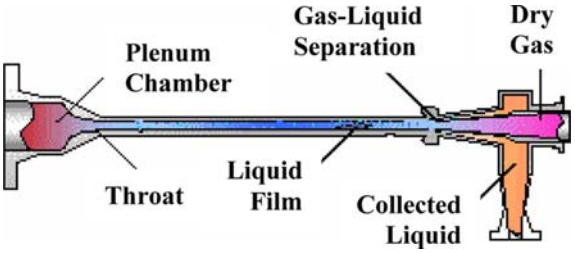

Fig. 2. Schematic diagram of a supersonic separator.

chamber) of 3S with a relatively low velocity and high pressure at near ambient temperature. A set of static vanes are positioned in the plenum chamber to induce massive swirling motion inside process fluid. The gas velocity increases to extremely high values (Ma>1) when it passes through the diffuser section of the Laval nozzle. Evidently, the fluid pressure drops erratically due to the huge transformation of potential energy into kinetic energy [36]. Moreover, the gas temperature dramatically is reduced across the Laval nozzle due to the adiabatic expansion phenomenon and all condensable species (e.g., water or heavy hydrocarbons) condense in extremely cooled supersonic section of the Laval nozzle.

Immense centrifugal accelerations (300,000-500,000 g) are anticipated due to the combination of supersonic flow of the gas stream and strong swirling motion induced by the plenum chamber. Under such extreme centrifugal forces, even submicron liquid droplets (water or condensable hydrocarbon species) will be thrown away towards the diffuser wall, leaving the 3S by a circumferential passage at collection point. The relatively liquid-free gas stream passes the separation point with extremely low temperature and pressure, while still retaining its very high velocity (Ma>1). Since higher operating pressure and temperature are desired for proper transmission of natural gas after separation of liquid phases from the gas stream, the fluid should be decelerated after collection point for pressure recovery purposes. This task can be achieved by using various scenarios such as normal shock wave occurrence or recruiting a second Laval nozzle as described in our previous article [16].

Note that the condensed water phase touches the 3S unit wall due to its higher density while the condensed liquid hydrocarbon flows over it. By proper adjustment of the liquid collection edge, any desired rate of liquid hydrocarbons can be separated (to retain the heating value of the exit gas stream), while removing the entire condensed water (to achieve the dehydration standard of 7 lbs water per 1MMSCF dry natural gas [37]).

MATHEMATICAL MODEL (FROM ENTRANCE TO COLLECTION POINT)

Assuming steady state flow condition, the one-dimensional governing equations for multi-phase flow of a condensable stream over any differential segment of an incremental distance dx inside a converging-diverging nozzle can be summarized as follows.

1. Continuity

Assuming negligible area occupied by liquid droplets (the upcoming simulation results clearly shows that less than 0.02% of the flow are will be occupied by the gas phase), the continuity equation in each section can be written as:

$$\dot{m}_t = \dot{m}_L + \rho_G A U_G \tag{1}$$

where $\dot{m}_t$ is the total mass flow rate, $\dot{m}_L$ is the liquid mass flow rate, ρ_G is the gas phase density, A is the cross-sectional area of nozzle at any segment and U_G is the gas velocity. Differentiating Eq. (1) leads to:

$$\frac{d\rho_G}{\rho_G} + \frac{dA}{A} + \frac{dU_G}{U_G} + \frac{d\dot{m}_L}{\dot{m}_t - \dot{m}_L} = 0 \tag{2}$$

2. Momentum Equation

The one-dimensional momentum changes across each segment can be expressed as:

$$d[\dot{m}_G U_G + \dot{m}_L U_L] = -A dP - \frac{f A \rho_G U_G^2}{2 d_e} dx \tag{3}$$

where f is the friction factor and d_e is the hydraulic diameter. Assuming no slippage between the gas and liquid phases (U_G=U_L) and dividing Eq. (3) by (A×P), the momentum equation can be simplified and rearranged as:

$$\frac{dP}{P} = -\frac{f \rho_G U_G^2}{2P} \frac{dx}{d_e} - \frac{m_t U_G}{AP} \frac{dU_G}{U_G} \tag{4}$$

3. Equation of State

The Peng-Robinson equation of state (EOS) can be written as:

$$P = \frac{RT_G}{V_G - b} = \frac{a\alpha}{V_G(V_G + b) + b(V_G - b)} \tag{5}$$

where V_G is the specific volume of gas phase, and a, α and b are the Peng-Robinson parameters (which are presented in Appendix A). On differentiation and using $1/\rho_G$ instead of V_G, Eq. (5) becomes:

$$\frac{dP}{P} - X\frac{d\rho_G}{\rho_G} - Y\frac{dT_G}{T_G} = 0 \tag{6}$$

$$X = \frac{B_1 + 2B_2\rho_G + \rho_G \frac{dB_1}{d\rho_G} + \rho_G^2 \frac{dB_2}{d\rho_G}}{B_1 + B_2\rho_G}$$

$$Y = \frac{B_1 + B_2\rho_G + \rho_G T_G \frac{dB_2}{dT_G}}{B_1 + B_2\rho_G}$$

$$B_1 = \frac{1}{1 - b\rho_G}$$

$$B_2 = -\frac{a\alpha}{RT_G(1 + b\rho_G + b - b^2\rho_G)}$$

Evidently, all PR parameters depend on composition of both gas and liquid phases and may dramatically change along the entire length of 3S unit in the x direction. For this reason, such parameters should be updated after calculation of temperature, pressure and composition of both phases for each spatial increment. This issue is shown in Fig. 3.

4. Energy Equation

The energy equation for steady state adiabatic flow at any section can be written as:

$$d\left[\dot{m}_G\left(h_G + \frac{U_G^2}{2}\right) + \dot{m}_L\left(h_L + \frac{U_L^2}{2}\right)\right] = 0 \tag{7}$$

where h_G and h_L are the gas and liquid enthalpies, respectively. The change of enthalpy of the vapor phase can be expressed by:

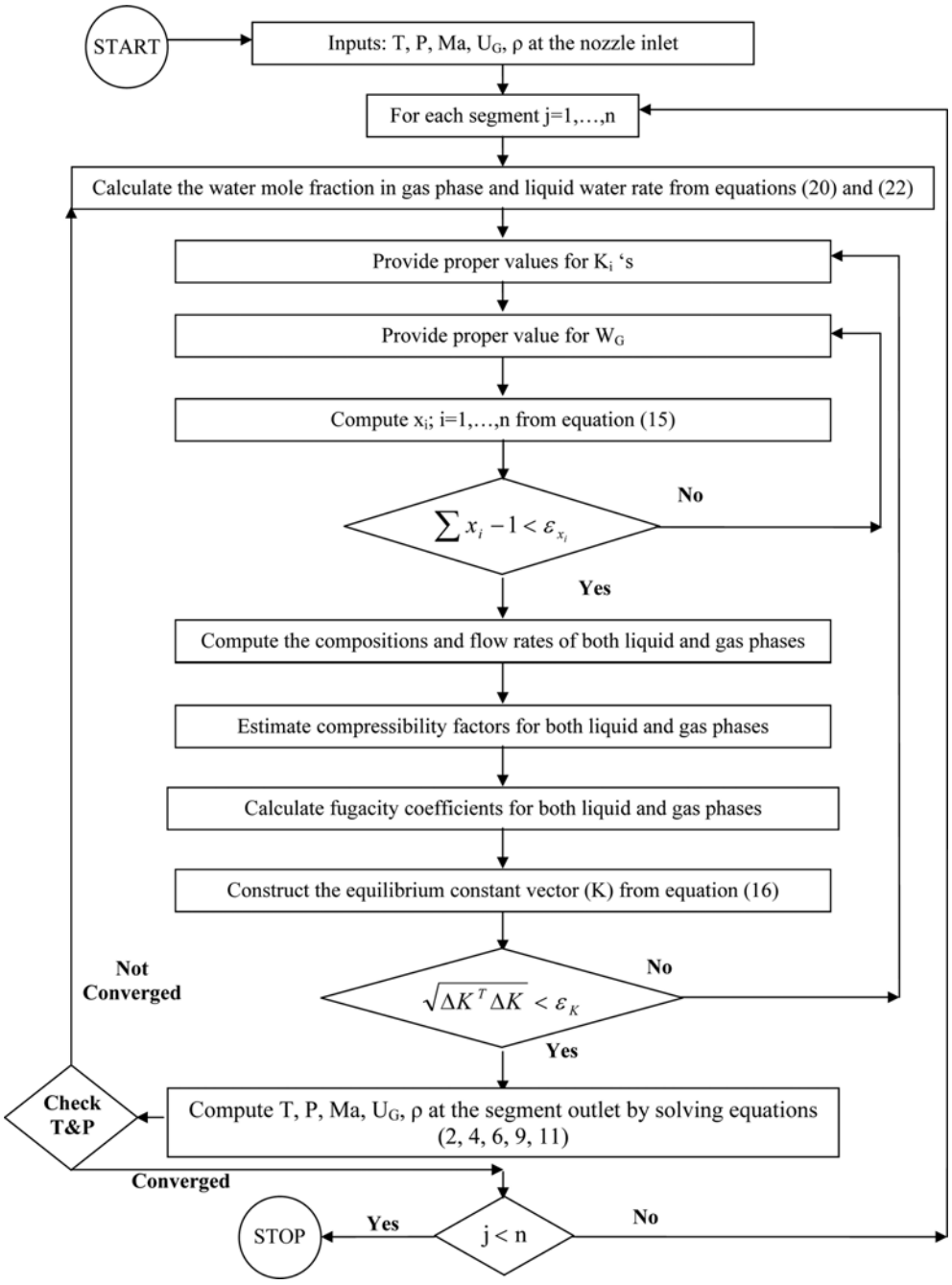

Fig. 3. Computation algorithm for calculation of operating parameters across each segment.

$$dh_G = \left(\frac{\partial h_G}{\partial T_G}\right)_P dT_G + \left(\frac{\partial h_G}{\partial P}\right)_{T_G} dP = c_P dT_G + \left[V_G - T_G\left(\frac{\partial V_G}{\partial T_G}\right)_P\right] dP = c_P dT_G + \frac{1}{\rho_G}\left(1 - \frac{Y}{X}\right) \tag{8}$$

Dividing Eq. (7) by $\dot{m}_t c_p T_G$ and replacing latent heat ($h_G - h_L$) with h_{fg} and using Eq. (8) for dh_G, leads to the following equation:

$$\frac{dT_G}{T_G} + \frac{P}{\rho_G c_p T_G}\left(1 - \frac{Y}{X}\right)\frac{dP}{P} + \frac{U_G^2}{c_p T_G}\frac{dU_G}{U_G} - \frac{h_{fg}}{C_p T_G}\frac{d\dot{m}_L}{\dot{m}_t} = 0 \tag{9}$$

5. Mach Number

The square of Mach number equation can be written as:

$$Ma^2 = \frac{U_G^2}{\gamma P/\rho_G} \tag{10}$$

where γ is the ratio of specific heats. Differentiating Eq. (10) and rearranging it leads to:

$$\frac{d(Ma^2)}{(Ma^2)} = 2\frac{dU_G}{U_G} + \frac{d\rho_G}{\rho_G} - \frac{dP}{P} \tag{11}$$

6. Prediction of Hydrocarbon Condensation Rate

In each segment, before solving fundamental governing equations, the liquid molar flow rate and concentration of components should be computed via phase equilibrium calculations. The total and components mole balances can be written as [38,39]:

$$\dot{m}_L + \dot{m}_G = \dot{m}_t \tag{12}$$

$$z_i \dot{m}_t = x_i \dot{m}_L + y_i \dot{m}_G \tag{13}$$

where z_i, x_i and y_i are the mole fractions of "i" component in the feed stream, liquid and gas phases, respectively. The mole fraction of liquid and gas phases are related to each other via equilibrium constant.

$$y_i = K_i x_i \tag{14}$$

Combination of Eqs. (12) to (14) and the fact that the sum of the mole fractions in each of liquid and gas phases is unity, results in:

$$x_i = \frac{\dot{m}_t z_i}{\dot{m}_t + \dot{m}_G (K_i - 1)} = 1 \tag{15}$$

The equilibrium constant can also be calculated from the following equation:

$$K_i = \frac{\phi_{Li}}{\phi_{gi}} \tag{16}$$

where ϕ_i is the fugacity coefficient and can be computed via Peng-Robinson equation of state (EOS):

$$\ln \phi_i = -\ln(z - B') + (z-1)B_i'' - \frac{A'}{2^{1.5}B'}(A_i'' - B_i'')\ln\left[\frac{z + (2^{1/2}+1)B'}{z - (2^{1/2}-1)B'}\right] \tag{17}$$

In this EOS, the z factor can be estimated by solving the following cubic equation:

$$z^3 - (1 - B')z^2 + (A' - 2B' - 3B'^2)z - (A'B' - B'^2 - B'^3) = 0 \tag{18}$$

Parameters, A', B', A_i'' and B_i'' are Peng-Robinson constants and should be computed for both liquid and gas phases separately, since each phase has its own composition.

For saturated systems, the above equation has three real roots for each of gas and liquid phases. The smaller root belongs to liquid phase compressibility factor, while the larger root corresponds to gas (vapor) compressibility factor. By substituting the values of z-factor for gas and liquid phases in Eq. (17), the fugacity coefficient of two phases can be easily computed.

As a first trial, a set of initial values should be assigned for all equilibrium constants, to compute an estimate of liquid and gas compositions for each segment. The following (Wilson) equation provides a convenient choice for this purpose [38]:

$$K_i = \frac{P_{ci}}{P}\exp\left(5.37(1+\omega_i)\left(1 - \frac{T_{ci}}{T}\right)\right) \tag{19}$$

where P_c, T_c and ω_i are the fluid critical pressure, temperature and acentric factor, respectively.

7. Prediction of Water Vapor Condensation Rate

Since water is immiscible in the mixture of liquid hydrocarbons, therefore, in the presence of water vapor the ordinary flash calculation should be performed by neglecting water as a component. The mole fraction of water vapor at each segment and before flash calculation can be computed via the following criteria:

$$y_w = \begin{cases} y_{win} & P_{win} < P_w^* \\ P_w^*/P_t & P_{win} \geq P_w^* \end{cases} \tag{20}$$

where P_{win} and y_{win} are the water vapor partial pressure and its mole fraction at the segment inlet, while P_w^* is the water vapor pressure at the corresponding segment temperature. By definition, the mole fraction of water vapor can be computed as:

$$y_w = \frac{\dot{m}_{Gw}}{\dot{m}_{Gw} + \dot{m}_{GHC}} \tag{21}$$

where $\dot{m}_{Gw}$ and $\dot{m}_{GHC}$ are the water vapor and hydrocarbon gas flow rates. Combination of Eqs. (20) and (21) provides $\dot{m}_{Gw}$ for known value of $\dot{m}_{GHC}$ at inlet condition. Afterwards, the condensed liquid water rate can be computed via simple mole balance at each segment as:

$$\dot{m}_{Lw} = \dot{m}_{tw} - \dot{m}_{Gw} \tag{22}$$

Fig. 3 illustrates the complete computational algorithm used for multi-component simulation of Laval nozzle of 3S unit during the condensation of water and hydrocarbon species.

REAL CASE STUDIES DESCRIPTION

Two different real case studies are presented in this section. The first one belongs to the methane-rich sweetened natural gas produced in the Khangiran gas refinery, which does not provide appreciable condensation of heavier hydrocarbons inside the Laval nozzle while sufficiently dehydrates the gas stream upon passing through 3S unit. The second case study involves the South Pars sweetened natural gas, which contains relatively large amounts of heavy hydrocarbons. Evidently, both water and hydrocarbon phases condense inside the Laval nozzle, which creates a more challenging case for multi-component simulation.

1. Case 1: Khangiran Natural Gas Refinery

Table 1 provides the composition of the Khangiran gas refinery sweetened natural gas on a carbon dioxide-free basis. The CO2 is excluded because its existence has several effects on the overall performance of the 3S unit. It can condense at extremely low temperatures and moderately high pressures around the collection point. Furthermore, the uncondensed CO2 can dissolve in condensed water and severely affect the corresponding equilibria, which greatly increases the complexity of the entire modeling. For simplicity and as a first trial, the CO2 free basis system was considered. The dry

Table 1. The sweetened Khangiran refinary natural gas composition (on a carbon dioxide free basis and saturated with water vapor)

Component	Mole fraction
Methane	0.9839
Ethane	0.0066
Propane	0.0007
Iso-Butane	0.0003
n-Butane	0.0003
Iso-Pentane	0.0004
n-Pentane	0.0004
n-Hexane & heavier	0.0012
Water vapor	0.0013
Nitrogen	0.0049

Table 2. Nozzle parameters

Parameter	Unit	Value
Inlet radius	m	0.0513
Inlet area	m^2	0.0083
Throat radius	m	0.05
Throat area	m^2	0.0079
Outlet radius	m	0.0808
Outlet area	m^2	0.0205
Nozzle (converging) length	m	0.1
Diffuser (diverging) length	m	0.7

natural gas is initially saturated with water vapor at 315 K and 64.9 atm using conventional steam tables.

At the present time, five adsorption dehumidification units are used to dry around 55MMSCMD (≈1942 MMSCFD) of such sweetened gas produced at the peak capacity of Khangiran gas refinery gas treating units (GTUs). Each unit consists of four adsorption towers, packed with two grades of silica gels. Each tower has around 2.5 meters diameter and more than 12 meters height. At each instance, two towers undergo the unsteady state adsorption process while the third and fourth ones are used for cooling and heating purposes. The present highest capacity of each dehumidification unit at the peak condition is around 11MMSCMD. Considering the future expansions of Khangiran GTU's, each adsorption dehumidification units is assumed to be replaced by a supersonic separation system of 13.4 MMSCMD. Table 2 provides the converging - diverging (Laval) nozzle geometries of such a 3S unit which can be used to control both hydrocarbon and water dew points. Evidently, such a 3S unit can easily outperform the conventional adsorption dehumidification units while occupying much smaller space, even with all its auxiliary equipment (e.g., pre- and post-cyclone separators and hydrate prevention system).

Each 1 MMSCF of the dried natural gas should contain less than seven pounds of water vapor. The initial saturated gas at 315 K contains around 60 pounds of water vapor per 1 MMSCF of wet gas. Therefore, more than 88 percent of the water vapor content of saturated gas should be removed to meet the above standard value. On the other hand, as shown in Table 1, the sweetened natural gas is actually free of heavy hydrocarbon. At the present time, the gross heating value (GHV) of Khangiran sweetened natural gas is around 34,700 kJ/SCM, which is the lowest heating value in the entire Middle-East region. Further separation of C_2^+ components will lead to extremely lower heating values, which would not be desirable. Therefore, only water dew point correction will be achieved in this case study.

In the second real case study, a typical South Pars sweetened wet gas stream is used to demonstrate the successful performance of 3S unit on simultaneous water and hydrocarbon dew point corrections.

2. Case 2: South Pars Natural Gas Refineries

Table 3 presents the composition of South Pars natural gas field sweetened on a carbon dioxide-free basis and saturated with water vapor at 297 K and 67.1 atm.

At the present time, the South Pars refineries include ten operating phases. Each phase contains two adsorption dehumidification units to dry around 25MMSCMD (≈883 MMSCFD) sweetened gas described in Table 3. Each dehydration unit consists of three adsorption towers, packed with two grades of silica gels. At each instance, two towers undergo the adsorption process, while the third one is cooled after a heating cycle. Evidently, each dehumidification unit dries around 12.5MMSCMD. Such large drying facilities can be avoided by replacing them with two parallel supersonic separators for each phase. Table 2 provides the corresponding nozzle geometries for each 3S unit which can receive around 13.1 MMSCMD wet sweetened natural gas. The saturated feed gas at 297 K contains around 20 pounds of water vapor per 1 MMSCF of wet gas. To achieve the standard value (7 pounds water vapor per 1 MMSCF dried gas), around 65 percent of the water content of the wet gas should be removed.

Table 3. South pars sweetened natural gas compositions (on a carbon dioxide free basis and saturated with water vapor)

Component	Mole fraction
Methane	0.8748
Ethane	0.0559
Propane	0.0204
Iso-Butane	0.0035
n-Butane	0.0053
Iso-Pentane	0.0014
n-Pentane	0.0012
n-Hexane & heavier	0.0014
Water vapor	0.0004
Nitrogen	0.0357

Due to the relatively large concentrations of heavy hydrocarbons available in the sweetened South Pars natural gas stream, simultaneous condensation of the both water and hydrocarbon phases will occur. Our in-house simulation package considers this issue and computes the water vapor and all hydrocarbon species concentration profiles across the entire length of supersonic separator.

SIMULATION RESULTS

The detailed algorithm of section 2 is applied to both case studies described in the previous section. The corresponding simulation results regarding water and/or hydrocarbon dew point corrections

Table 4. Carbon dioxide free basis composition of Khangiran dried natural gas (prior to collection point)

Component	Mole fraction
Methane	0.98845
Ethane	0.00625
Propane	0.00032
Iso-Butane	0.00003
n-Butane	0.00001
Iso-Pentane	2.4e-6
n-Pentane	1.1e-6
n-Hexane & heavier	2.2e-7
Water vapor	1.2e-9
Nitrogen	0.00493

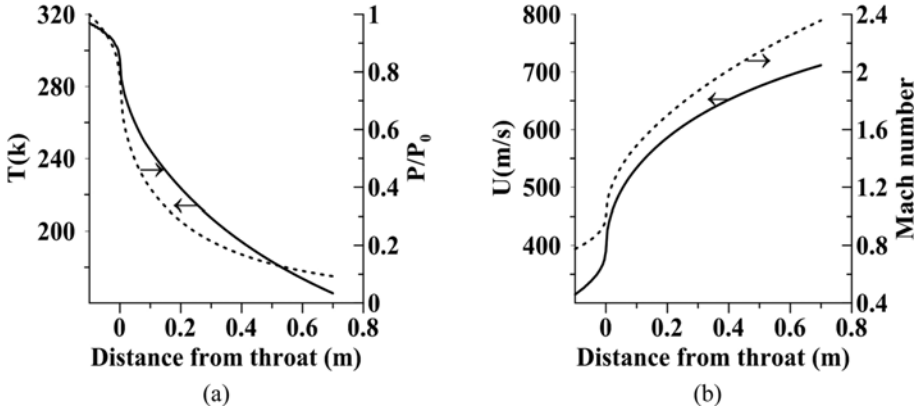

Fig. 4. Simulation results of case1 for distribution of operating parameters across Laval nozzle.
(a) Temperature and pressure distribution, (b) Velocity and Mach number distribution

via using 3S unit are provided in the following sections.

1. Case 1

As previously mentioned, water dew point correction (in the absence of heavy hydrocarbons condensation) was the main objective of our first case study. Table 4 provides the mole fractions of all species at the outlet of Laval nozzle before collection point is reached. As can be seen, large amounts of heavy hydrocarbons are condensed at the prevailing outlet temperature and pressure (167 K and 6.5 atm.). Evidently, such large heavy hydrocarbon condensation rates are not desirable. As mentioned earlier, by proper adjustment of the liquid collection edge, any desired rate of liquid hydrocarbons can be separated (to retain the heating value of the exit gas stream).

Fig. 4(a) illustrates the corresponding simulation results for the computed temperature and pressure profiles across the Laval nozzle. Fluid encounters extremely low temperatures at the collection point, which provides appropriate conditions for the condensation of many hydrocarbons and water vapor. Evidently, at excessively low temperatures of around 170 K (≅−100 °C) and in the presence of liquid condensed water, the situation is ideal for the formation of methane hydrate even at moderate pressures of around 10 atmospheres. Fortunately, this troubling phenomenon does not occur due to exceptionally small residence time inside 3S unit (0.002 to 0.005 seconds), which is not sufficient for successful hydrate formation.

Fig. 4(b) shows similar velocity and Mach number distributions along the Laval nozzle. Note that the outlet Mach number reaches to more than 2.3, which is responsible for such large drop in temperature and pressure of the gas and liquid streams. After separation of liquid phases from the gas stream, the fluid should be decelerated for pressure recovery purposes via normal shock wave or any other facility [16]. Decreasing the Mach number and velocity will increase both gas pressure and temperature which would be desirable for proper transmission purposes. The current modeling uses an isentropic model to simulate the flow behavior prior to normal shock position.

Since Khangiran sweetened natural gas contains small amounts of heavy hydrocarbons, further condensation of hydrocarbon species (C_2^+) reduces its poor heating value, which is not actually desirable. Therefore, the sole reason for using a 3S unit is to reduce the water content of the gas stream to standard value of 7 lbs water per one

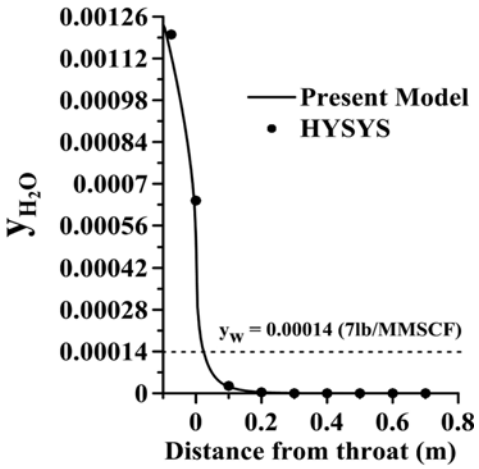

Fig. 5. Water concentration profile across Laval nozzle shows that the collection point can be moved towards throat location.

MMSCF of dried gas. As clearly shown in Fig. 5, only five percent of the diffuser length is required to achieve the standard value (y_w= 0.00014). So, the collection point can be situated at about 10 percent of the diffuser length from throat location. The remaining length can be used for pressure recovery purposes. Interestingly, at this new location of the collection point, the fluid temperature and pressure are around 270 K and 32 atm. respectively. Evidently, at such condition, negligible amounts of existing hydrocarbons will be condensed.

As mentioned earlier, HYSYS simulation software cannot provide any prediction for various operating condition profiles (e.g., T and P) across the 3S Laval nozzle. The initial feed entering the 3S unit is flashed via HYSYS software at the computed temperature and pressure profiles calculated by the procedure shown in Fig. 3. The HYSYS predictions are then compared with our present model in Figs. 5 to 7 and 9 to 10. In the absence of experimental data, these comparisons of the results obtained from two independent methods are used for validation purposes.

Fig. 6 shows the computed distribution of cumulative liquid flow rate inside the Laval nozzle. As can be observed, a small kink can be detected. The pre-kink rise belongs to the condensation of water

vapor while the second post-kink rise represents the condensation of heavy hydrocarbons. A second notable point in this figure is the change of its slope across the Laval nozzle. Before the start of hydrocarbon condensation (pre-kink location), the slope tends to zero because the water content of the gas stream drops quickly. This phenomenon cannot be observed for hydrocarbon phase, because the lighter hydrocarbons start to condense as the temperature drops additionally. Two assumptions in mathematical modeling were made, which were negligible area occupied by liquid droplets and no slippage between the gas and liquid phases. As mentioned in the pervious section, each supersonic separator for the first case study will receive 13.4 MMSCMD wet gas, which has a real volume of about 1.13 MMCMD (13.08 CMS) at the end of Laval nozzle (T≅170 K, P≅7 atm, see Fig. 4(a)). From Fig. 6, the maximum condensation rate is around 0.0425 kgmole/s, which corresponds to a volumetric flow rate of about 0.0027 CMS. Therefore, the condensed phase (both water and hydrocarbon) always occupies less than 0.02% of the total cross sectional area of the Laval nozzle. Furthermore, the gas velocity at the end of nozzle is about 700 m/s (as shown in Fig. 4(b)), and therefore these extremely small and submicron liquid droplets will be carried directly by the gas stream with the same velocity, which verifies the no-slip condition.

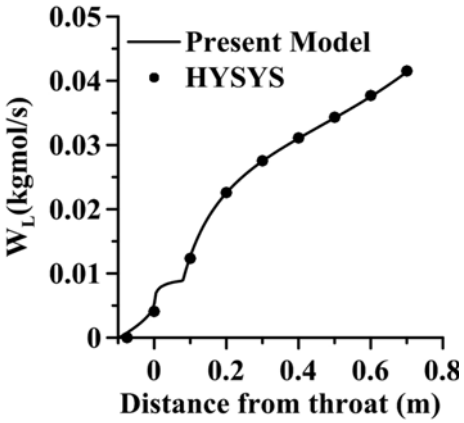

Fig. 6. Simulation results of case1 for distribution of cumulative liquid flow rate.

Fig. 7 provides concentration distributions for all condensable species and methane along the Laval nozzle. Clearly, the reductions in the slope of mole fractions for heavier hydrocarbons are larger than lighter hydrocarbons. Furthermore, the mole fraction of methane increases due to the condensation of other species. The heating

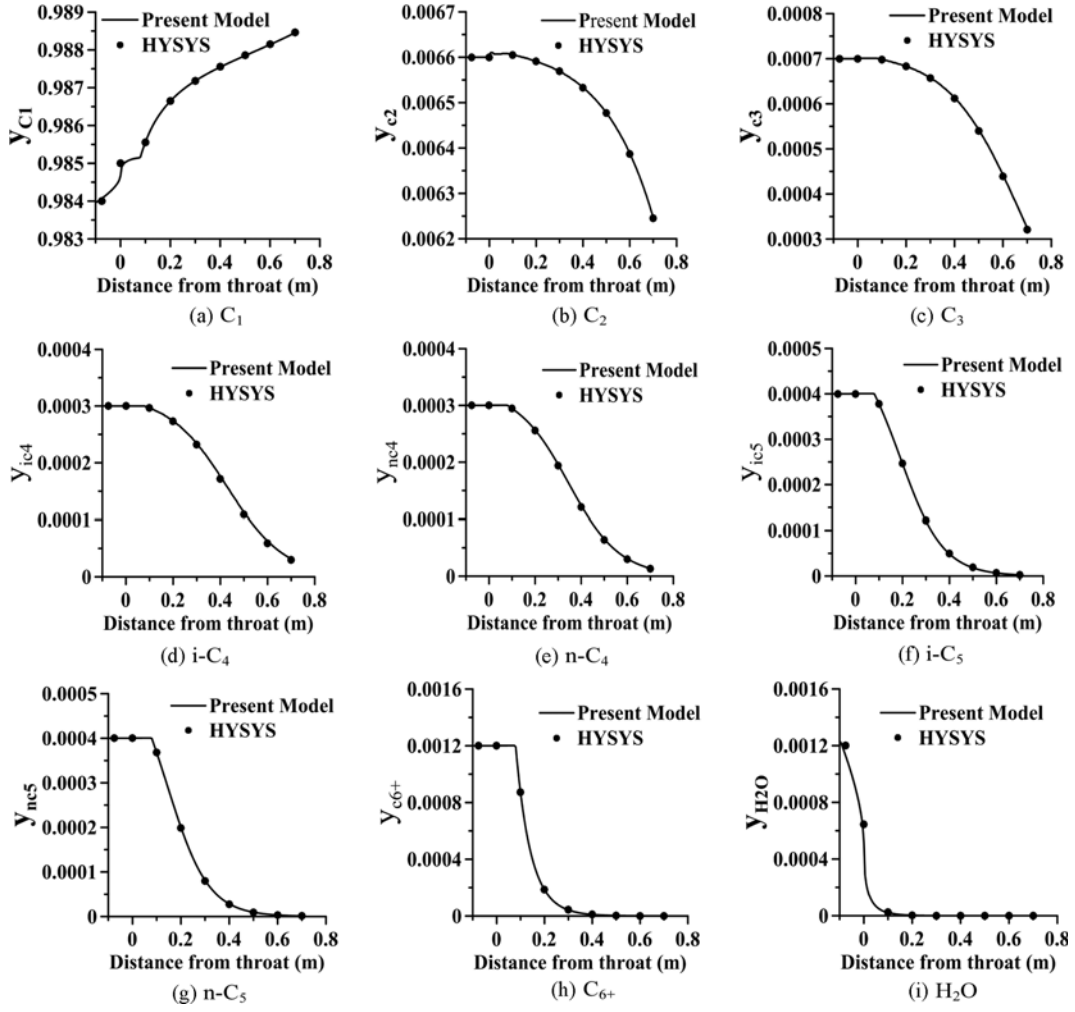

Fig. 7. Simulation results of case1 for distribution of components mole fraction across Laval nozzle.

Table 5. Carbon dioxide free basis composition of south pars dried natural gas before collection point of 3S unit

Component	Mole fraction
Methane	0.91888
Ethane	0.03996
Propane	0.00298
Iso-Butane	0.00010
n-Butane	0.00007
Iso-Pentane	3.4e-6
n-Pentane	1.5e-6
n-Hexane & heavier	1.7e-7
Water vapor	1.8e-8
Nitrogen	0.03800

value of any natural gas depends on its heavy hydrocarbons content. On the other hand, large quantities of heavy hydrocarbons may cause problems in the gas transportation system due to creation of two-phase flow. Therefore, in an ideal situation, maximum heating value of the natural gas should be preserved while avoiding the creation of two phase region. Since the natural gas heating value of the first case study was relatively small, the water vapor content should be reduced to its permissible value without appreciable condensation of heavy hydrocarbons. One of the advantages of supersonic separators is selective removal of impurities via suitable adjustment of the collection point. This selective removal is based on the different condensation points. As can be seen in Fig. 7, the water vapor content reaches under 7 lbs/MMSCF of dried gas (y_w=0.00014) at around 0.1 m distance from throat. At this point, almost all of heavy hydrocarbons remain in the natural gas stream as vapor, and therefore separation of water vapor without condensation of heavy hydrocarbons can be achieved.

2. Case2

As reported in Table 3, the South Pars sweetened natural gas contains relatively large amounts of heavier hydrocarbons (C_2^+). Therefore, in addition to water dew point correction, the separation of heavy hydrocarbons is also important. Table 5 illustrates the simulation results for species mole fractions at the outlet of Laval nozzle. The water vapor mole fraction is reduced much lower than its permissible value. Furthermore, the appreciable decrease in mole fractions of C_2^+ components indicates that large amounts of these heavier hydrocarbons are also condensed inside the diffuser section. As previously, since the water vapor content of natural gas reaches its desired standard value just after the throat location, therefore the actual length of the entire Laval nozzle should be selected based on the preferred C_2^+ concentrations.

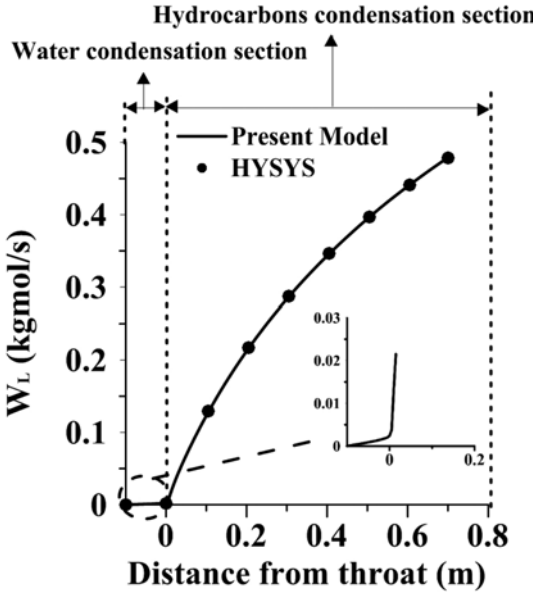

Fig. 9. Simulation results for cumulative liquid flow rate across laval nozzle.

Fig. 8(a) illustrates the temperature and pressure distributions along both diverging and converging sections of the Laval nozzle when the South Pars sweetened natural gas enters the 3S unit. Fig. 8(b) also depicts similar profiles for the corresponding fluid axial velocity and gas Mach number. As in case 1, the 3S unit provides extremely low temperature and pressures necessary for condensation of both hydrocarbons and water vapor phases. The large Mach number at the outlet condition is responsible for these large temperature and pressure drops. It should be emphasized that the same nozzle geometry is used for both case studies. Different inlet conditions (e.g.,

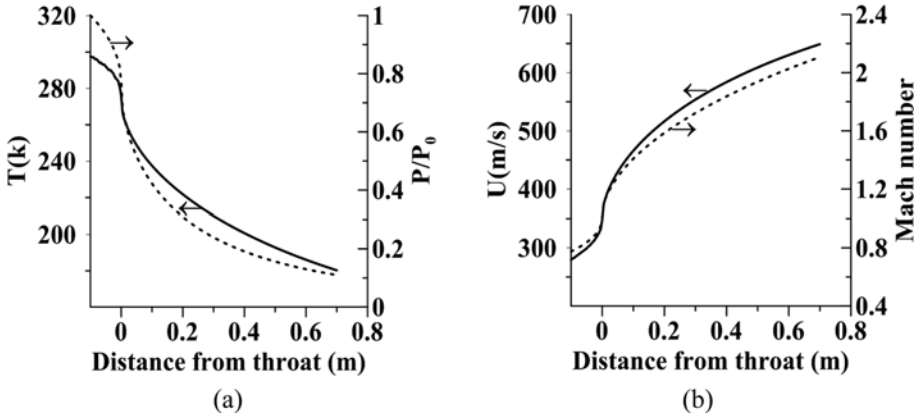

Fig. 8. Simulation results for various operating parameters profiles across Laval nozzle.
(a) Temperature and pressure distributions, (b) Velocity and Mach number distributions

pressure and temperature) lead to different velocity and Mach number distributions, even when same nozzle geometry was used. To achieve a unit Mach number at the throat location, the inlet gas velocity of cases1 and 2 should be 315 m/s and 280 m/s, respectively.

Fig. 9 presents the cumulative liquid flow rate distribution along the Laval nozzle. Similar to the previous case, the water vapor initially condenses and leads to a sudden rise in liquid flow rate profile. However, the large condensation rate of heavy hydrocarbons suppresses the water vapor condensation and the sudden rise due water liquefaction is not distinguishable. This point is demonstrated in the magnified view of Fig. 9. Relatively large amounts of condensed liquid hydrocarbons can be collected due to higher concentration of heavy hydrocarbons at the inlet stream. Although liquid phase flow is much higher than in the previous case, it still occupies less than 0.013% of the cross sectional area. Each supersonic separator receives 13.1 MMSCMD wet gas, which has a real volume of about 1.22MMCMD (14.12 CMS) at the end of nozzle condition (T≅180 K, P≅6.71 atm, refer to Fig. 8(a)). Fig. 9 shows that the maximum condensation rate is around 0.475 kgmole/s, which occupies about 0.00175 CMS. Therefore, the maximum liquid flow rate occupies less than 0.013% of the total cross sectional area at the end of Laval nozzle.

Fig. 10 provides the distributions of various species mole fractions along the Laval nozzle of 3S unit. As mentioned, in contrast to the previous case study, hydrocarbon dew point correction is also important in this case because of the relatively large amounts of heavier hydrocarbons available in the inlet natural gas stream. So, the collection point should be positioned at the proper point where the outlet natural gas stream has the required heating value. Evidently, based on such distributions of species concentrations, a successful design of 3S unit can be achieved to provide the desired concentrations of water vapor and heavier hydrocarbons at the outlet condition.

It should be emphasized that HYSYS software can provide proper predictions only when correct temperatures and pressures across the entire 3S Laval nozzle are used. It is not capable of finding any temperature or pressure distribution. Figs. 11 and 12 clearly demonstrate this issue. In these figures, cases 1 and 2 represent the simulations results obtained with our present model in the presence and absence of condensation, respectively. In other words, the equilibrium calculations are performed in each step for case 1 while it was neglected in case 2. As can be seen, the HYSYS software may provide unrealistic results when inadequate temperature and pressure distributions are used as the inputs. This issue will be more severe when the condensation rate is relatively high (e.g., South Pars data) when compared to other cases, such as Khangiran gas which has a much smaller condensation rate.

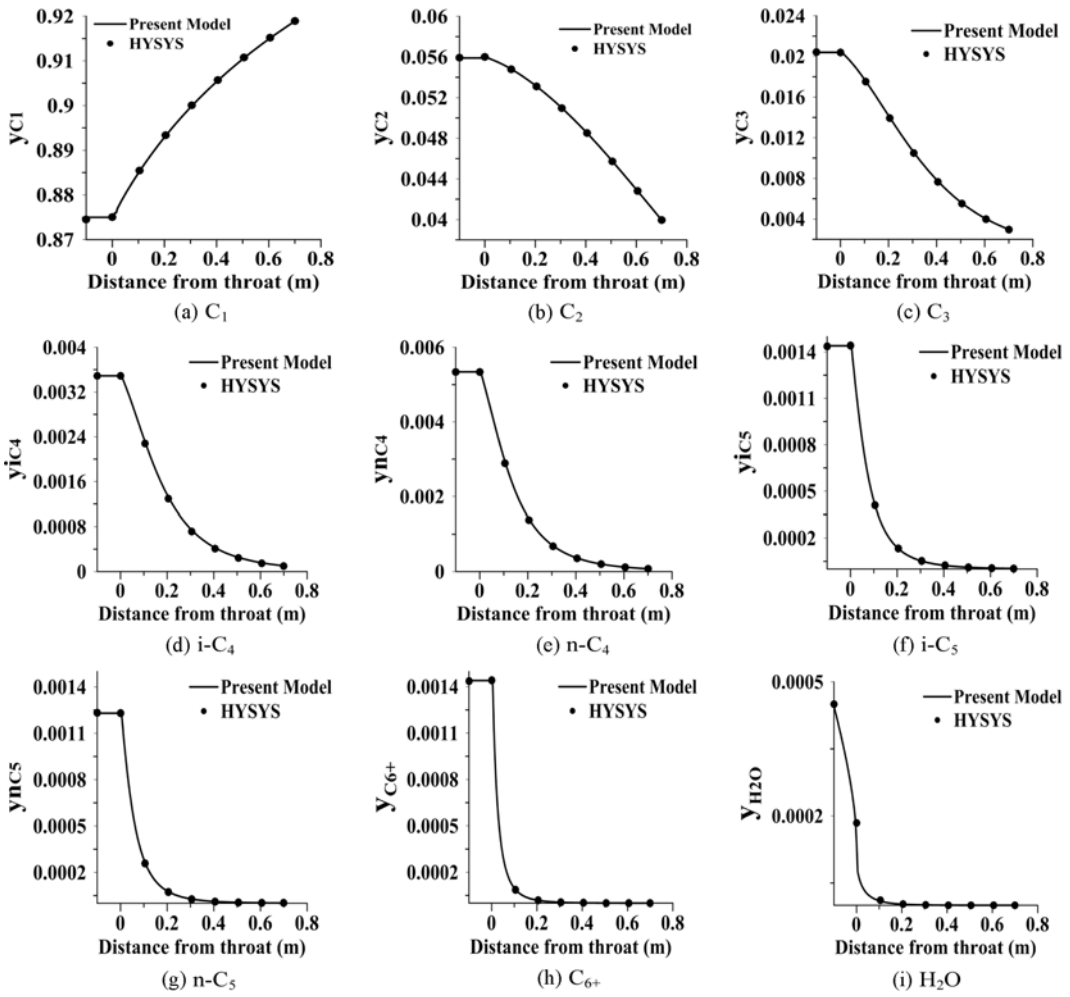

Fig. 10. Simulation results for various components mole fractions profiles across Laval nozzle.

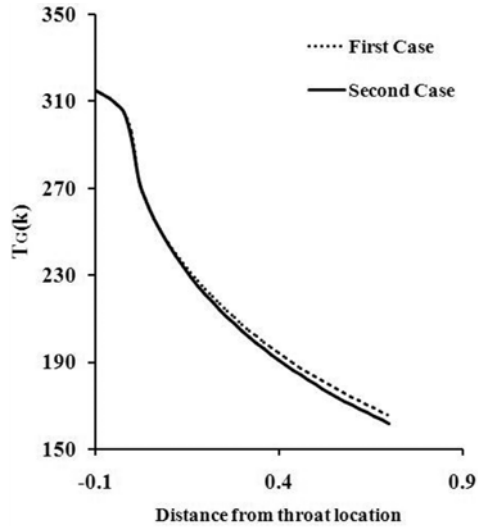

(a)

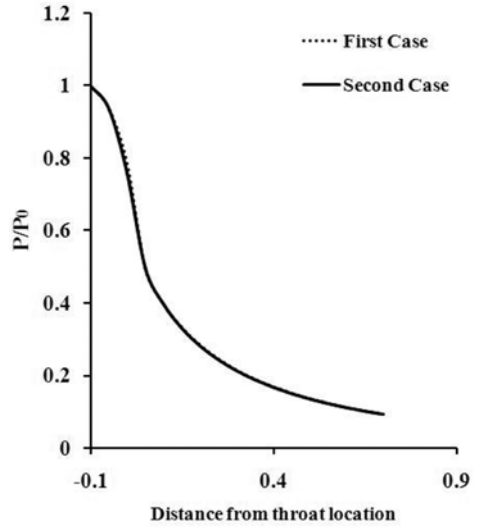

(b)

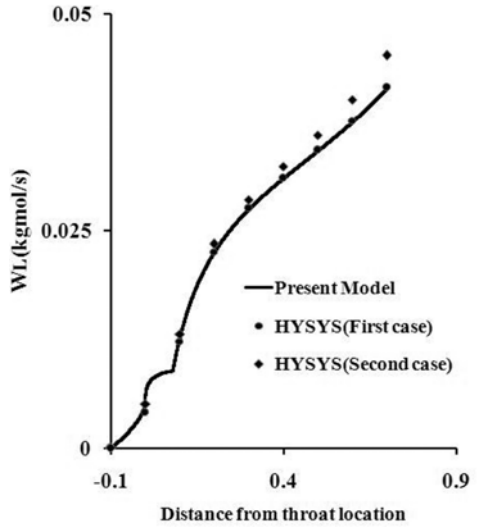

(c)

Fig. 11. The effect of latent heat on distribution of various parameters for Khangiran gas.
(a) Temperature, (b) Pressure, (c) Liquid flow rate

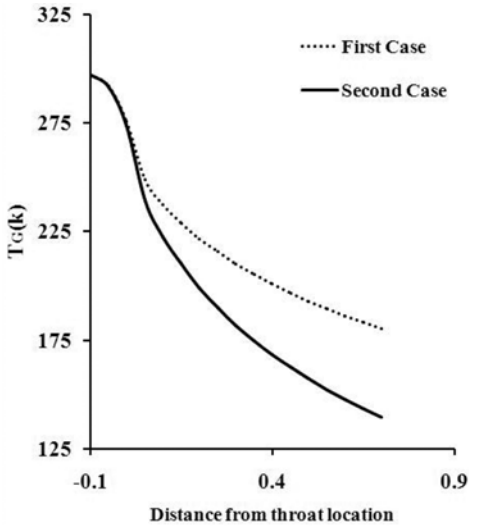

(a)

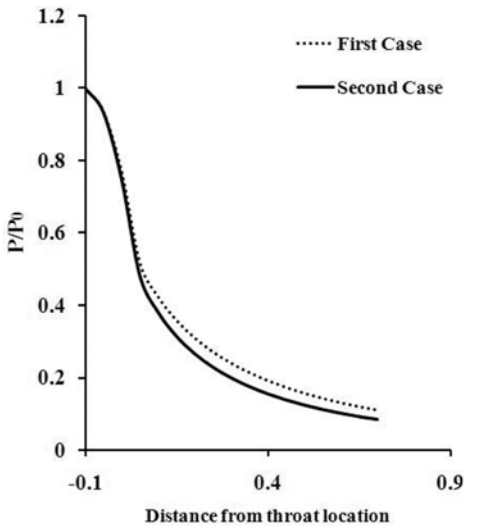

(b)

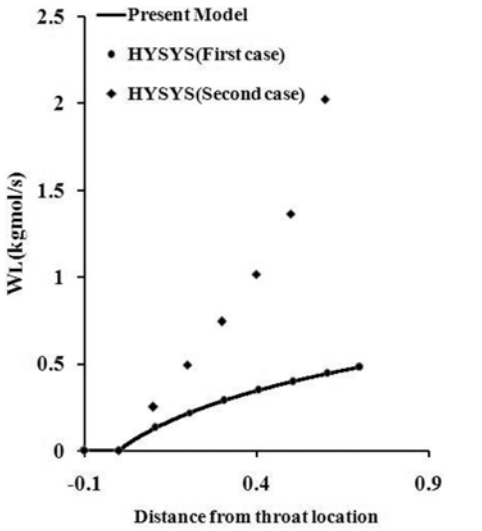

(c)

Fig. 12. The effect of latent heat on distribution of various parameters for South Pars gas.
(a) Temperature, (b) Pressure, (c) Liquid flow rate

CONCLUSION

Water and heavy hydrocarbon dew point corrections of natural gas streams are essential for safe transportation purposes and preserving their heating values. Supersonic separators can achieve both tasks with high reliability, minimal operating costs and small operational facilities requirements.

Despite the complexity of multi-component multiphase systems, the present approach recruited a combination of fundamental governing equations and phase equilibrium calculations to predict various operating conditions profiles and different components mole fractions distributions along the entire length of 3S unit Laval nozzle for multi-component and multi-phase system. The simulation results indicate that the 3S units can be used successfully to remove almost the entire water content of natural gas for two real case studies. It was also clearly shown that the 3S units are able to successfully reduce the heavier hydrocarbon concentrations to the desired values necessary for practical applications. The simulation results were validated by resorting to other independent methods such as HYSYS simulation software.

Finally, the existence of carbon dioxide has several effects on the overall performance of the 3S unit. It can condense at extremely low temperatures and moderately high pressures around collection point. Furthermore, the uncondensed CO2 can dissolve in condensed water and severely affect the corresponding equilibria which greatly increases the complexity of the entire modeling. For simplicity, and as a first trial, the CO2 free basis system was considered. It can be investigated as an independent factor in our future work.

NOMENCLATURE

a, A', A''_i, b, B', B''_i: Peng-Robinson parameters
A : area [m^2]
B_1, B_2: function of temperature, density and PR parameters in EOS
C_p : specific heat at constant pressure [j/kgmol k]
d_e : hydraulic diameter [m]
dx : incremental distance [m]
F : friction factor
H : enthalpy [j/kg]
h_{fg} : latent heat [j/kgmol]
K_i : equilibrium constant of component i
$\dot{m}$: mass flow rate [kgmol/s]
Ma : mach number
P : pressure [Pa]
P^* : saturation pressure [Pa]
P_c : critical pressure [Pa]
R : gas constant
T : temperature [k]
T_c : critical temperature [k]
U : velocity [m/s]
V_G : specific volume of gas phase
X : function of temperature and density in equation of state
x_i : mole fraction in liquid phase
Y : function of temperature and density in equation of state
y_i : mole fraction in gas phase
Z : compressibility factor
z_i : components mole fraction in the inlet
ρ : density [kgmol/m^3]
ω : acentric factor
ϕ : fugacity coefficient
γ : ratio of specific heats

Subscripts
G : gas phase
HC : hydrocarbon
i : component i
in : inlet
L : liquid phase
t : total
W : water

Superscripts
* : saturation

REFERENCES

1. M. Betting and H. D. Epsom, *World Oil Mag*., **254**, 197 (2007).
2. A. Karimi and M. A. Abdi, *Chem. Eng. Process*., **48**, 560 (2009).
3. P. B. Machado, J. G. M. Monteiro, J. L. Medeiros, H. D. Epsom and O. Q. F. Araujo, *J. Nat. Gas. Sci. Eng*., **6**, 43 (2012).
4. F. Okimoto and J. M. Brouwer, *World Oil Mag*., **223**, 89 (2002).
5. V. I. Alferov, L. A. Baguirov, L. Dmitriev, V. Feygin, S. Imaev and J. R. Lace, *Oil Gas J.*, **103**, 53 (2005).
6. P. Schinkelshoek and H. Epsom, in Proc. *GPA 87th Annual Convention*, TX (2008).
7. H. Liu, Z. Liu, Y. Feng, K. Gu and T. Yan, *Chin. J. Chem. Eng*., **13**, 9 (2005).
8. E. Jassim, M. A. Abdi and Y. Muzychka, *Pet. Sci. Technol*., **26**, 1757 (2008).
9. E. Jassim, M. A. Abdi and Y. Muzychka, *Pet. Sci. Technol*., **26**, 1773 (2008).
10. M. M. Malyshkina, *High Temp*., **46**, 69 (2008).
11. M. M. Malyshkina, *High Temp*., **48**, 244 (2010).
12. C. Wen, X. Cao and Y. Yang, *Chem. Eng. Process*., **50**, 644 (2011).
13. C. Wen, X. Cao, Y. Yang and J. Zhang, *Chem. Eng. Technol*., **34**, 1575 (2011).
14. C. Wen, X. Cao, Y. Yang and W. Li, *Energy*, **37**, 195 (2012).
15. C. Wen, X. Cao, Y. Yang and J. Zhang, *Adv. Powder Technol*., **23**, 228 (2012).
16. M. Ghanbari Mazidi, A. Shahsavand and B. M. Vaziri, *J. Pet. Technol*., In press.
17. F. Bakhtart and M. T. Mohammadi Tochai, *Int. J. Heat Fluid Flow*, **2**, 5 (1980).
18. A. Guha and J. B.Young, *I Mech E Conf. Publ*., 167 (1991).
19. G. Cinar, B. S. Yilbas and M. Sunar, *Int. J. Multiphase Flow*, **23**, 1171 (1997).
20. A. J. White and M. J. Hounslow, *Int. J. Heat Mass Transfer*, **43**, 1873 (2000).
21. S. Dykas, *Task Q*., **5**, 519 (2001).
22. A. G. Gerber and M. J. Kermani, *Int. J. Heat Mass Transfer*, **47**, 2217 (2004).
23. M. R. Mahpeykar and A. R. Teymourtash, *Sci. Iran., Trans. B.*, **11**, 269 (2004).
24. Y. Yang and Sh. Shen, *Int. Commun. Heat Mass Transfer*, **36**, 902

(2009).
25. S. Dykas and W. Wroblewski, *Int. J. Heat Mass Transfer*, **53**, 933 (2012).
26. G. Cinar, B. S. Yilbas and M. Sunar, *Int. J. Multiphase Flow*, **23**, 1171 (1997).
27. Q. F. Ma, D. P. Hu, J. Z. Jiang and Z. H. Qiu, *Int. J. Comput. Fluid Dyn.*, **23**, 221 (2009).
28. Q. F. Ma, D. P. Hu, J. Z. Jiang and Z. H. Qiu, *Int. J. Comput. Fluid Dyn.*, **24**, 29 (2010).
29. B. Lingling, L. Zhongliang, L. Hengwei, J. Wenming, Z. Ming and Z. Jian, *Sci. China Technol. Sci.*, **53**, 435 (2010).
30. S. H. Rajaee Shooshtari and A. Shahsavand, *J. Sep. Purif. Technol.*, **116**, 458 (2013).
31. S. D. Mohaghegh, *J. Pet. Technol.*, **57**, 8691 (2005).
32. S. Zendehboudi, M. A. Ahmadi, A. Bahadori, A. Shafiei and T. Babadagli, *Can. J. Chem. Eng.*, **91**, 1325 (2013).
33. G. Zahedi, A. R. Fazlali, S. M. Hussein, G. R. Pazuki and L. Sheikhattar, *J. Pet. Sci. Eng.*, **68**, 218 (2009).
34. A. Shahsavand and A. Ahmadpour, *Comput. Chem. Eng.*, **29**, 2134 (2005).
35. A. Shahsavand and M. Pourafshari Chenar, *J. Membr. Sci.*, **297**, 59 (2007).
36. B. M. Vaziri, A. Shahsavand, H. Rashidi and M. G. Mazidi, *in Proc. 13th Iranian National Chemical Engineering Cong. & 1st Int. Regional Chemical and Petroleum Engineering*, Kermanshah, Iran (2010).
37. A. Kohl and R. Nielsen, *Gas Purification*. 5th Ed., Gulf Pub. Co., Houston, Texas (1997).
38. T. H. Ahmed, *Hydrocarbon phase behavior*, 1st Ed., Gulf Pub. Co., USA (1989).
39. W. D. Mccain, *The properties of petroleum fluid*, 2nd Ed., Pennwell Pub. Co., Tlsu, Oklahoma, USA (1990).

APPENDIX A. PARAMETERS OF PENG-ROBINSON EQUATION OF STATE

The Peng-Robinson equation of state is presented in Eq. (A1) [34]:

$$P=\frac{RT_G}{V_G-b}-\frac{a_T}{V_G(V_G+b)+b(V_G-b)} \tag{A1}$$

Where V_G is the specific volume of gas phase, and a_T and b are the Peng-Robinson parameters and can be calculated from following equations using mixing rule.

$$b=\sum_j y_j b_j \tag{A2}$$

$$b_j=0.07780\frac{RT_{cj}}{P_{cj}} \tag{A3}$$

$$a_T=\sum_i\sum_j y_i y_j (a_{Ti}a_{Tj})^{1/2}(1-\delta_{ij}) \tag{A4}$$

$$a_{ij}=a_{ci}\alpha_j \tag{A5}$$

$$a_{ci}=0.45724\frac{R^2T_{cj}^2}{P_{cj}} \tag{A6}$$

$$\alpha_j^{1/2}=1+(0.37464+1.54226\omega_j-0.26992\omega_j^2)(1-T_{rj}^{1/2}) \tag{A7}$$

In the above equations, y_i is the mole fraction of component "i", T_c is critical temperature, P_c is critical pressure, δ_{ij} is binary interaction parameter between components "i" and "j", T_r is reduced temperature and ω_j is acentric factor.

In this EOS, fugacity coefficient, z factor and their parameters can be computed by following equations:

$$\ln\phi_i=-\ln(z-B')+(z-1)B_i''-\frac{A'}{2^{1.5}B'}(A_i''-B_i'')\ln\left[\frac{z+(2^{1/2}+1)B'}{z-(2^{1/2}-1)B'}\right] \tag{A-8}$$

$$z^3-(1-B')z^2+(A'-2B'-3B'^2)z-(A'B'-B'^2-B'^3)=0 \tag{A-9}$$

$$A'=\frac{a_T P}{R^2T^2} \tag{A10}$$

$$B'=\frac{bP}{RT} \tag{A11}$$

$$B_i''=\frac{b_i}{b} \tag{A12}$$

$$A_j''=\frac{1}{a_T}\left(2a_{Tj}^{1/2}\sum_i y_i a_{Ti}^{1/2}(1-\delta_{ij})\right) \tag{A13}$$

APPENDIX B. PHYSICAL PROPERTIES OF COMPONENTS

B.1. Heat capacities:

$$C_p(\text{j/kmolk})=C_1+C_2\left(\frac{C_2/T(k)}{\sinh(C_3/T(k))}\right)^2+C_4\left(\frac{C_5/T(k)}{\cosh(C_5/T(k))}\right)^2 \tag{B-1}$$

Table B.1. Values of heat capacities constants

Component	$C_1\times10^{-5}$	$C_2\times10^{-5}$	$C_3\times10^{-3}$	$C_4\times10^{-5}$	C_5	T_{min} (k)	T_{max} (k)
Methane	0.333	0.7993	2.0869	0.4160	991.96	50	1500
Ethane	0.4033	1.3422	1.6555	0.7322	752.87	200	1500
Propane	0.5192	1.9245	1.6265	1.1680	723.6	200	1500
n-Butane	0.7134	2.4300	1.6300	1.5033	730.42	200	1500
i-Butane	0.6549	2.4776	1.5870	1.5750	−706.99	200	1500
n-Pentane	0.8805	3.0110	1.6502	1.8920	747.6	200	1500
i- Pentane	0.7460	3.2650	1.5450	1.9230	666.7	200	1500
n-Hexane	1.0440	3.5230	1.6946	2.3690	761.6	200	1500
Water	0.3336	0.2679	2.6105	0.0890	1169	100	2273.15

B.2. Critical constants and Acentric factors:

Table B.2. Values of heat critical constants and acentric factors

Component	T_c (k)	$P_c \times 10^{-6}$ (Pa)	Acentric factor
Methane	190.564	4.59	0.011
Ethane	305.32	4.85	0.098
Propane	369.83	4.21	0.149
n-Butane	425.12	3.77	0.197
i-Butane	408.14	3.62	0.177
n-Pentane	469.7	3.36	0.251
i- Pentane	460.43	3.37	0.226
n-Hexane	507.6	3.04	0.304
Water	647.13	21.94	0.343

B.3. Latent heats:

B.3.1. Hydrocarbons latent heats:

$$H_{fg}(\text{j/kmol}) = C_1 \times (1 - T_r)^{C_2 + C_3 \times T_r + C_4 \times T_r \times T_r} \tag{B-2}$$

$$T_r = \frac{T}{T_c} \tag{B-3}$$

B.3.2. Water latent heat:

$$H_{fg}(\text{j/kmol}) = -1.08T(\text{k})^3 + 913.8T(\text{k})^2 - 3 \times 10^5 T(\text{k}) + 8.078 \times 10^7$$

$$248\text{k} < T < 313\text{k} \tag{B-4}$$

Table B.3. Values of latent heats constants

Component	$C_1 \times 10^{-7}$	C_2	C_3	C_4	T_{min} (k)	T_{max} (k)
Methane	1.0194	0.26087	−0.14694	0.22154	90.69	190.56
Ethane	2.1091	0.60646	−0.55492	0.32799	90.35	305.32
Propane	2.9209	0.78237	−0.77319	0.39246	85.47	369.83
n-Butane	3.6238	0.8337	−0.82274	0.39613	134.86	425.12
i-Butane	3.1667	0.3855	0	0	113.54	408.14
n-Pentane	3.9109	0.38681	0	0	143.42	469.7
i- Pentane	3.7700	0.3952	0	0	113.25	460.43
n-Hexane	4.4544	0.39002	0	0	177.83	507.6